Desalination and Water Treatment
www.deswater.com

doi: 10.5004/dwt.2019.24101

155 (2019) 162–167
July

Optimization of the fluidized bed for crystallization process: seed fluidization study

Ke Jiang[a,b,*], Kanggen Zhou[b]

[a]*Changsha Environmental Protection College, Changsha, 410004, China. Tel. +86 13874913813; Fax: +86 0731 85622912; email: j_k8663661@126.com (K. Jiang)*
[b]*School of Metallurgy and Environment, Central South University, Changsha, 410083, China, email: zhoukg63@163.com*

Received 18 September 2018; Accepted 8 March 2019

ABSTRACT

To investigate the influence of seed fluidization on the operation and design of the fluidized bed for crystallization process, the relationships between the seed mass, seed size (L), the minimum fluidization velocity (U_{mf}), and the terminal velocity (U_t) were determined using quartz sand. The results show that the equation $U_{mf} = 7.40 \times 10^{-4} \times L^{0.51}$ can be used to predict the minimum fluidization velocity at the seed size range of 176.5–844.6 μm. The equation $U_t = 7.72 \times 10^{-6} \times L^{1.38}$ can be used to predict the terminal velocity at the seed size range of 109.7–763.1 μm. The pressure difference of the FBR can be used to estimate the seed mass. The design of the sedimentation zone and the adjustment of the reflux flow are possible ways to control the fluid velocity between the minimum fluidization velocity and the terminal velocity, allowing the seed to maintain fluidization without running out of the fluidized bed.

Keywords: Design; Superficial velocity; Fluidization; Quartz sand

1. Introduction

As a simple and effective technique, chemical precipitation has been widely used for wastewater treatment. Contaminants, including fluoride, ammonia, phosphorus, and heavy metals are transformed to stable precipitations, and then removed by solid-liquid separation [1–4]. The precipitations generated during the process are fine in particle size, low in quality, and are non-reusable, making it need to be disposed with high costs [5]. Therefore, the fluidized bed reactors (FBR) are developed based on the crystallization process [6–9]. The precipitations with large particle size can easily be separated, as the seed retention time is prolonged in the FBR [10,11].

In recent years, studies have been conducted to determine crystallization conditions. The factors reaction pH, reaction molar ratio, and supersaturation are considered to be the main factors influencing the crystallization process [12–16]. In addition, the seed also plays an important role in inducing the crystallization of the precipitations [8,17,18]. The design and operation of the FBR are the key in determining system performance. It is necessary to control the fluid velocity between the minimum fluidization velocity and the terminal velocity, so that the seed can be kept suspended in a fluidized state. However, studies on the optimization of the FBR, as well as the relationships between the seed fluidization and the FBR, are rarely conducted.

The density and size are the main factors influencing the fluidization state of seed. The seeds in the crystallization process generally involve $MgNH_4PO_4$, $CaCO_3$, CaF_2, and SiO_2, with the density of 1.71, 2.71, 3.18, and 2.58 g/cm^3, respectively [19–22]. The seeds of $MgNH_4PO_4$, $CaCO_3$, and CaF_2 with a wide size range are difficult to purchase or prepare. To determine the fluidization properties of the seeds in the crystallization process, the commercial quartz sand (SiO_2) was used as the seed material for simulation. Series fluidization experiments were conducted to determine the

* Corresponding author.

relationships between the seed and the fluid velocity in the FBR. The influence of seed mass and seed size on the minimum fluidization velocity and the terminal velocity were investigated. Following, the optimal fluidization parameters of the seed were obtained and utilized to guide the design and optimization of the FBR.

2. Materials and methods impact

2.1. Fluidized bed and process description

The commercial quartz sand was used as the seed material. The schematic of the FBR is shown in Fig. 1. The poly methyl methacrylate fluidized bed consisted of a mixing zone, and a fluidization zone (inner diameter = 50 mm; height = 800 mm). A liquid distributor was set up between the mixing zone and the fluidization zone to maintain good dispersion of the influent and the seed. The seed was added from the top of the fluidized bed. The tap water was flowed to the bottom of the fluidized bed by a magnetic pump. The pressure difference was measured by a U-shaped manometer. The solid samples were obtained from the seed outlet.

2.2. Experiment analysis

The minimum fluidization flow (F_{mf}) was determined when all seeds kept fluidization. The minimum fluidization velocity (U_{mf}) was defined as:

$$U_{mf} = \frac{F_{mf}}{S} \tag{1}$$

where S is the cross-sectional area within the fluidization zone of the FBR.

The terminal flow (F_t) was determined when seeds ran out of the outlet. The terminal velocity (U_t) was defined as:

$$U_t = \frac{F_t}{S} \tag{2}$$

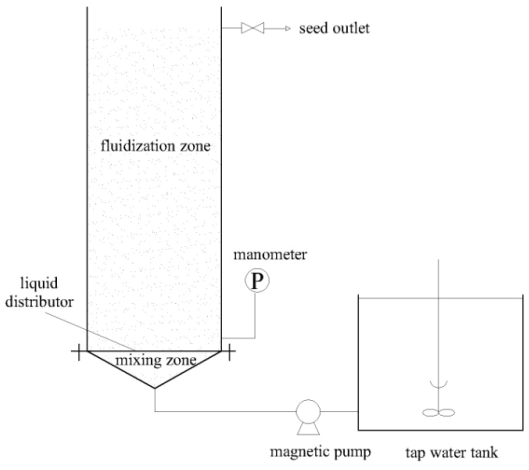

Fig. 1. Schematic diagram of the fluidized bed for the fluidization experiment.

The seed was analyzed using a scanning electron microscopy (SEM, JSM 6360LV). The krummbein diameter (L_k) of the seed was measured by the computer programme Smile View based on the SEM image. The area mean diameter was defined as the particle size of the seed (L), which was calculated as:

$$L = \left(\sum L_k^{\,2}\right)^{1/2} \tag{3}$$

2.3. Theory calculation

The pressure difference (ΔP) was calculated as [23]:

$$\Delta P = \frac{(1-\varepsilon)\times(m_p - m_l)}{S} \tag{4}$$

where ε is the porosity of bed, m_p is the mass of solid, m_l is the mass of the liquid with the same volume of the solid.

The minimum fluidization velocity (U_{mf}) was calculated as [23]:

$$\mathrm{Re}_{mf} = \left[(33.7)^2 + 0.0408\frac{L^3\rho_l(\rho_p-\rho_l)g}{\eta^2}\right]^{\frac{1}{2}} - 33.7 \tag{5}$$

$$\mathrm{Re}_{mf} = \frac{U_{mf}L\rho_l}{\eta} \tag{6}$$

where ρ_p and ρ_l are the density of solid and liquid, respectively; Re_{mf} is the Reynolds number; η is the viscosity of the liquid. In this study, $\rho_p = 2.58\times10^3$ kg/m^3, $\rho_l = 1\times10^3$ kg/m^3, $\eta = 1\times10^{-3}$ N·s·m^{-2}.

The terminal velocity (U_t) was calculated as [23]:

$$U_t = \frac{L^2[(\rho_p-\rho_l)g]}{18\mu_l} \quad \mathrm{Re}_t < 0.05 \tag{7}$$

$$U_t = \left[\frac{4}{3}\frac{L(\rho_p-\rho_l)}{C_D\rho_l}\right]^{0.5} \quad 0.05 < \mathrm{Re}_t < 2000 \tag{8}$$

$$U_t = 1.74\left[\frac{L(\rho_p-\rho_l)}{K_3\rho_l}\right]^{0.5} \quad 2000 < \mathrm{Re}_t < 200000 \tag{9}$$

where Re_t is the Reynolds number; μ_f is the kinematic viscosity of the liquid, C_D is the drag coefficient.

3. Results and discussion

3.1. Characteristic of the seed fluidization

3.1.1. Influence of the seed mass on fluidization

Experiments were conducted at a seed size of 8–20 mesh. Fig. 2 shows the influence of the superficial velocity on the pressure difference of the FBR as a function of the seed mass.

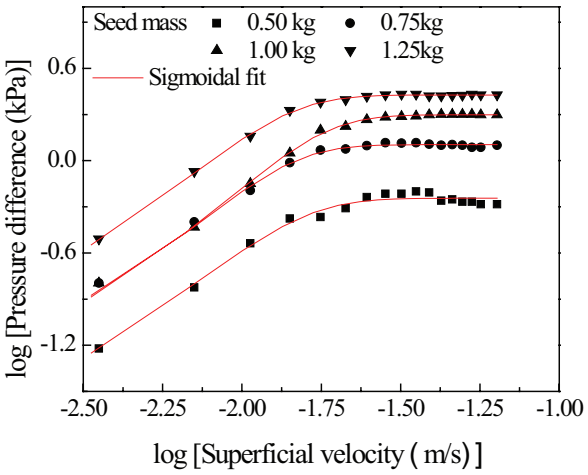

Fig. 2. Influence of the superficial velocity on the pressure difference of the FBR as a function of the seed mass.

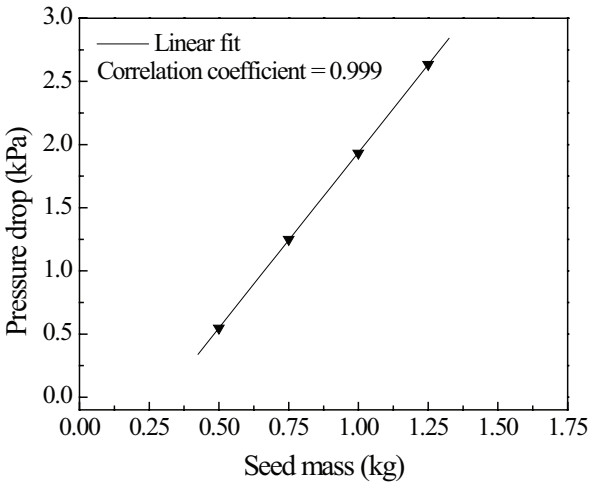

Fig. 3. The relationship between the seed mass and the pressure difference of the FBR.

The pressure difference of the FBR remains stable when all seeds maintain fluidization. The minimum fluidization velocities (U_{mf}) are 0.025, 0.025, 0.028, and 0.025 m/s at the seed mass of 0.5–1.25 kg. Therefore, the minimum fluidization velocity maintains stability with increasing seed mass.

According to Eqs. (5) and (6), the minimum fluidization velocity is determined by seed size, seed density, and solution properties. Seed mass has no influence on the minimum fluidization velocity, which is consistent with the experiment results.

However, the pressure difference of the FBR increases with increasing seed mass, as shown in Fig. 3. The relationship between the seed mass and the pressure difference fits well with the linear model, which is consistent with Eq. (4) and previous results [15]. Therefore, the pressure difference of the FBR can be used to estimate the seed mass, and the operation state of the FBR can be indirectly monitored.

3.1.2. Influence of the seed size on fluidization

Experiments were conducted at a seed mass of 0.5 kg. Fig. 4 shows the influence of the superficial velocity on the pressure difference of the FBR as a function of the seed size. Fig. 5 shows the influence of the seed size on the terminal velocity.

As shown in Fig. 4, the minimum fluidization velocities (U_{mf}) are 0.011, 0.017, 0.021, and 0.028 m/s at the seed size of 176.5, 320.3, 602.8, and 844.6 μm, respectively. The minimum fluidization velocity increases with increasing seed size while the pressure difference of the FBR remains stable.

According to Eqs. (5) and (6), the minimum fluidization velocity in theory was predicted, as shown in Eq. (10) and Fig. 6.

$$U_{mf} = 7.40 \times 10^{-4} \times L^{0.51} \quad (10)$$

The linear correlation between the experimental and predicted values of U_{mf} is 0.985. Therefore, Eq. (10) can be used to predict the minimum fluidization velocity at the seed size range of 176.5–844.6 μm.

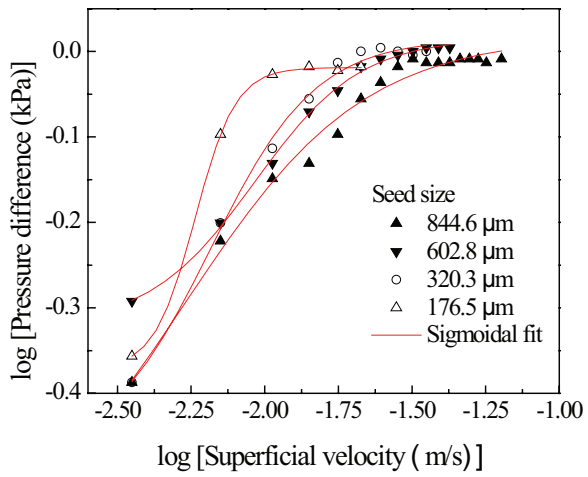

Fig. 4. Influence of the superficial velocity on the pressure difference of the FBR as a function of the seed size.

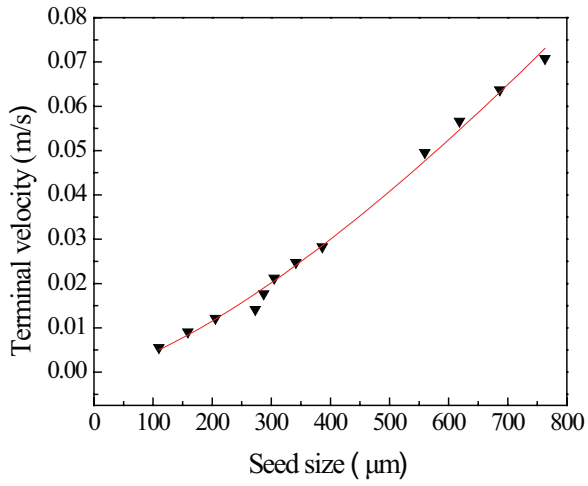

Fig. 5. Influence of the seed size on the terminal velocity.

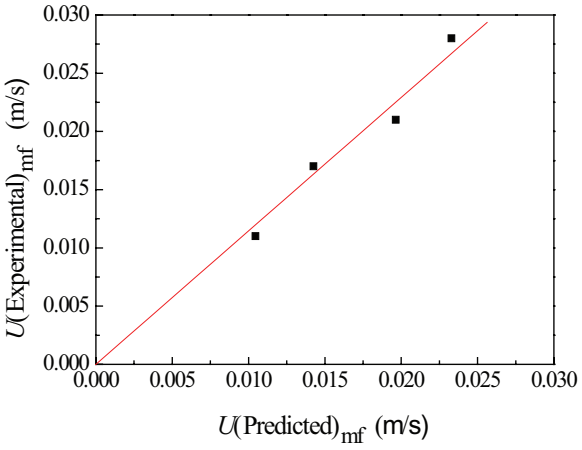

Fig. 6. Parity graph for the predicted and experimental values of the fluidization velocity of the seed.

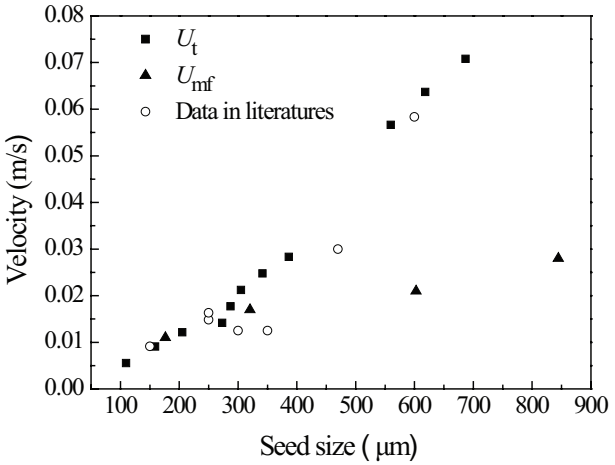

Fig. 7. Comparison of the minimum fluidization velocity and the terminal velocity obtained in the experiments and the normal operational velocity in the literatures.

As shown in Fig. 5, the terminal velocity increases with increasing seed size. The relationship between U_t and L can be described as follows according to Eqs. (7)–(9):

$$U_t = \beta L^{\alpha} \quad 0.5 < \alpha < 2 \tag{11}$$

The data in Fig. 5 are fitted to Eq. (11), as shown in Eq. (12).

$$U_t = 7.72 \times 10^{-6} \times L^{1.38} \tag{12}$$

The correlation coefficient is 0.993, indicating that the experimental data match well with the fitting equation. Therefore, Eq. (12) can be used to predict the terminal velocity at the seed size range of 109.7–763.1 μm.

3.2. Optimization of the FBR

The optimal operational velocity should be kept between the minimum fluidization velocity and the terminal velocity, so that the seeds are in the fluidized state and are retained in the FBR. Fig. 7 shows the comparison of the minimum fluidization velocity and the terminal velocity obtained in the experiments, in addition to the normal operational velocity in the literatures [8,24–26]. It can be observed that the data in the literatures match well with what is found within this experiment. Therefore, Fig. 7 can be used to guide the determination of the operational velocity of the FBR with a more wide range of seed size. During the crystallization process of the FBR, the influent flow needs to be adjusted for the change in seed size and seed mass to preserve the operational velocity in the optimal range of Fig. 7.

Furthermore, the cross-sectional area (S) and the diameter (D) of the FBR can be calculated as follows:

$$S = \frac{\pi D^2}{4} = \frac{F_{in}}{U_{in}} \tag{13}$$

where F_{in} is the influent flow of the FBR, U_{in} is the operational velocity which can be obtained in Fig. 7.

In our previous work [15], both fine seeds and large seeds exist in the FBR during the crystallization process. In order to determine the fluidization characteristics of the seeds with a wide size distribution, experiments were conducted with the seed size of 8–325 mesh, as shown in Fig. S1 (See supplemental material). The pressure difference of the FBR first increases and then decreases with increasing superficial velocity. This result is different from the seed with a narrow size distribution in Fig. 2. As shown in Fig. 7, the minimum fluidization velocity of the fine seeds is close to the terminal velocity. With increasing influent flow on operation, the large seeds are gradually fluidized, while the fine seeds run out of the FBR. This leads to the loss of the fine seeds and a decrease in the pressure difference. Therefore, the operation range of influent flow is difficult to control. In order to prevent the loss of the fine seeds, two possible methods can be suggested:

1. A sedimentation zone with an enlarged diameter can be set above the fluidization zone of the FBR. The fluid velocity is reduced, thus allowing fine seeds to be kept in the FBR. The diameter of the sedimentation zone can be calculated by the fine seed size and the terminal velocity in Fig. 7.
2. A reflux pipeline can be set from the sedimentation zone to the influent inlet. Increasing the reflux flow can fluidize all the seeds, while the effluent velocity maintains stable. Therefore, the mass loss of the fine seeds can be effectively avoided.

Based on the suggestion above, we designed a laboratory-scale [15] and a pilot-scale fluidized bed reactor [10] for crystallization of CaF_2, respectively. The sedimentation and the reflux pipeline were both set in the reactors. The reflux flow and the bed pressure drop were adjusted according to the fluidization parameters of CaF_2 for better operation.

4. Conclusions

The fluidization properties of quartz sand seed were studied in a fluidized bed. The minimum fluidization velocity

and the terminal velocity of the seed were obtained by the fluidization experiment and the theory calculation. The main conclusions are as follows:

1. The minimum fluidization velocity maintains stability with increasing seed mass. The pressure difference of the FBR can be used to estimate the seed mass during the operation.
2. The minimum fluidization velocity and the terminal velocity are determined by seed size. The equation $U_{mf} = 7.40 \times 10^{-4} \times L^{0.51}$ can be used to predict the minimum fluidization velocity at the seed size range of 176.5–844.6 μm. The equation $U_t = 7.72 \times 10^{-6} \times L^{1.38}$ can be used to predict the terminal velocity at the seed size range of 109.7–763.1 μm.
3. To control the fluid velocity properly, the influent flow should be adjusted immediately according to the change of the seed size, the seed mass, the pressure difference of the FBR, the minimum fluidization velocity, and the terminal velocity.
4. To prevent loss of the fine seeds, the sedimentation zone and the reflux pipeline can be designed based on the minimum fluidization velocity and the terminal velocity.

Acknowledgments

This research was supported by the Major Science and Technology Program of Hunan (NO. 2009FJ-1009).

References

[1] Ezzeddine, N. Meftah, A. Hannachi, Removal of fluoride from an industrial wastewater by a hybrid process combining precipitation and reverse osmosis, Desal. Wat. Treat., 55 (2015) 2618–2625.
[2] H. Huang, J. Liu, P. Zhang, D. Zhang, F. Gao, Investigation on the simultaneous removal of fluoride, ammonia nitrogen and phosphate from semiconductor wastewater using chemical precipitation, Chem. Eng. J., 307 (2017) 696–706.
[3] M. Cerrillo, J. Palatsi, J. Comas, J. Vicens, A. Bonmatí, Struvite precipitation as a technology to be integrated in a manure anaerobic digestion treatment plant–removal efficiency, crystal characterization and agricultural assessment, J. Chem. Technol. Biotechnol., 90 (2015) 1135–1143.
[4] N. Rostamnezhad, D. Kahforoushan, E. Sahraei, S. Ghanbarian, M. Shabani, A method for the removal of Cu (II) from aqueous solutions by sulfide precipitation employing heavy oil fly ash, Desal. Wat. Treat., 57 (2016) 17593–17602.
[5] K. Van den Broeck, N. Van Hoornick, J. Van Hoeymissen, R. de Boer, A. Giesen, D. Wilms, Sustainable treatment of HF wastewaters from semiconductor industry with a fluidized bed reactor, IEEE Trans. Semicond. Manuf., 16 (2003) 423–428.
[6] M.D.G. de Luna, R.R.M. Abarca, C.-C. Su, Y.-H. Huang, M.-C. Lu, Multivariate optimization of phosphate removal and recovery from aqueous solution by struvite crystallization in a fluidized-bed reactor, Desal. Wat. Treat., 55 (2015) 496–505.
[7] C. Huang, J.R. Pan, M. Lee, S. Yen, Treatment of high-level arsenic-containing wastewater by fluidized bed crystallization process, J. Chem. Technol. Biotechnol., 82 (2007) 289–294.
[8] C. Zhang, K.N. Xu, J.Y. Li, C.W. Wang, M. Zheng, Recovery of phosphorus and potassium from source-separated urine using a sluidized bed reactor: optimization operation and mechanism modeling, Ind. Eng. Chem. Res., 56 (2017) 3033–3039.
[9] P. Battistoni, R. Boccadoro, F. Fatone, P. Pavan, Auto-nucleation and crystal growth of struvite in a demonstrative fluidized bed reactor (FBR), Environ. Technol., 26 (2005) 975–982.
[10] K. Jiang, K.G. Zhou, Recovery and removal of fluoride from fluorine industrial wastewater by crystallization process: a pilot study, Clean Technol. Environ. Policy, 19 (2017) 2335–2340.
[11] J. Chung, E. Jeong, J.W. Choi, S.T. Yun, S.K. Maeng, S.W. Hong, Factors affecting crystallization of copper sulfide in fed-batch fluidized bed reactor, Hydrometallurgy, 152 (2015) 107–112.
[12] F.C. Ballesteros, A.F.S. Salcedo, A.C. Vilando, Y.H. Huang, M.C. Lu, Removal of nickel by homogeneous granulation in a fluidized-bed reactor, Chemosphere, 164 (2016) 59–67.
[13] Y.J. Shih, R.R.M. Abarca, M.D.G. de Luna, Y.H. Huang, M.C. Lu, Recovery of phosphorus from synthetic wastewaters by struvite crystallization in a fluidized-bed reactor: effects of pH, phosphate concentration and coexisting ions, Chemosphere, 173 (2017) 466–473.
[14] Y. Shen, Z.L. Ye, X. Ye, J. Wu, S. Chen, Phosphorus recovery from swine wastewater by struvite precipitation: compositions and heavy metals in the precipitates, Desal. Wat. Treat., 57 (2016) 10361–10369.
[15] K. Jiang, K.G. Zhou, Y.C. Yang, H. Du, Growth kinetics of calcium fluoride at high supersaturation in a fluidized bed reactor, Environ. Technol., 35 (2014) 82–88.
[16] M.D.G. de Luna, L.M. Bellotindos, R.N. Asiao, M.C. Lu, Removal and recovery of lead in a fluidized-bed reactor by crystallization process, Hydrometallurgy, 155 (2015) 6–12.
[17] Z. Liu, Q. Zhao, L. Wei, D. Wu, L. Ma, Effect of struvite seed crystal on MAP crystallization, J. Chem. Technol. Biotechnol., 86 (2011) 1394–1398.
[18] C.C. Su, L.D. Dulfo, M.L.P. Dalida, M.C. Lu, Magnesium phosphate crystallization in a fluidized-bed reactor: effects of pH, Mg:P molar ratio and seed, Sep. Purif. Technol., 125 (2014) 90–96.
[19] D. Crutchik, J.M. Garrido, Struvite crystallization versus amorphous magnesium and calcium phosphate precipitation during the treatment of a saline industrial wastewater, Water Sci. Technol., 64 (2011) 2460–2467.
[20] S.K. Bhatia, D.D. Perlmutter, Effects of the product layer on the kinetics of the CO_2-lime reaction, AIChE J., 29 (1983) 79–86.
[21] A.G. Dijkman, J. Tak, J. Arends, Fluoride deposited by topical applications in enamel, Caries Res., 16 (1982) 147–155.
[22] R. Aldaco, A. Irabien, P. Luis, Fluidized bed reactor for fluoride removal. Chem. Eng. J., 107 (2005) 113–117.
[23] M.S. Guo, H.Z. Li, Handbook of Fluidization, Chemical Industry Press, Beijing, 2008.
[24] R. Aldaco, A. Garea, A. Irabien, Calcium fluoride recovery from fluoride wastewater in a fluidized bed reactor, Water Res., 41 (2007) 810–818.
[25] R. Aldaco, A. Garea, A. Irabien, Particle growth kinetics of calcium fluoride in a fluidized bed reactor, Chem. Eng. Sci., 62 (2007) 2958–2966.
[26] V.T. Costodes, A.E. Lewis, Reactive crystallization of nickel hydroxy-carbonate in fluidized-bed reactor: fines production and column design, Chem. Eng. Sci., 61 (2006) 1377–1385.

Supplementary material

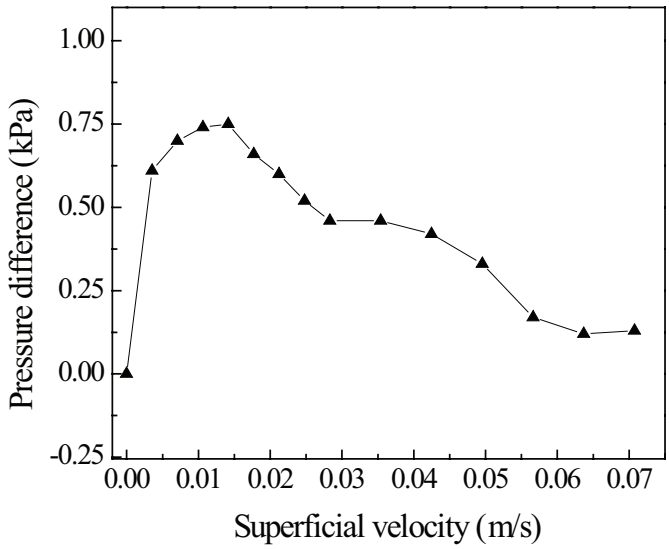

Fig. S1. Influence of the superficial velocity on the pressure difference of the FBR with the seed of a wide size distribution. Seed composition: 8–20 mesh, 0.1 kg; 20–30 mesh, 0.1 kg; 30–60 mesh, 0.1 kg; 60–100 mesh, 0.1 kg; 100–200 mesh, 0.1 kg; 200–325 mesh, 0.1 kg.